



# Molecular modeling studies of vascular endothelial growth factor receptor tyrosine kinase inhibitors using QSAR and docking

Juan Du<sup>a</sup>, Beilei Lei<sup>a</sup>, Jin Qin<sup>a</sup>, Huanxiang Liu<sup>b</sup>, Xiaojun Yao<sup>a,\*</sup>

<sup>a</sup> Department of Chemistry, Lanzhou University, Lanzhou 730000, China

<sup>b</sup> School of Pharmacy, Lanzhou University, Lanzhou 730000, China

## ARTICLE INFO

### Article history:

Received 18 August 2008

Received in revised form 17 October 2008

Accepted 20 October 2008

Available online 5 November 2008

### Keywords:

Vascular endothelial growth factor receptor

2 (VEGFR-2)

KDR inhibitor

CoMFA

CoMSIA

Docking

## ABSTRACT

The vascular endothelial growth factor (VEGF) and its receptor tyrosine kinases VEGFR-2 or kinase insert domain receptor (KDR) are attractive targets for the development of novel anticancer agents. In the present work, comparative molecular field analysis (CoMFA) and comparative molecular similarity indices analysis (CoMSIA) were performed on a series of selective inhibitors of KDR. Docking studies were performed to explore the binding mode between all of the inhibitors and the KDR and produce the bioactive conformation of each compound in the whole dataset. Two conformer-based alignment strategies were employed to construct reliable 3D-QSAR models. The docked conformer-based alignment strategy gave the best 3D-QSAR models. The best CoMFA and CoMSIA models gave a cross-validated coefficient  $q^2$  of 0.546 and 0.715, non-cross-validated  $r^2$  values of 0.936 and 0.961, predicted  $r^2$  values of 0.673 and 0.797, respectively. The information obtained from molecular modeling studies were very helpful to design some novel selective inhibitors of KDR with desired activity.

© 2008 Elsevier Inc. All rights reserved.

## 1. Introduction

Angiogenesis, the process of blood vessel sprouting, generating new capillaries from existing vasculature, is a normal process for organ development during embryogenesis, wound healing and the menstrual cycle [1,2]. Abnormal regulation of angiogenesis has been found to be involved in the pathogenesis of several disorders including inflammation [3], rheumatoid arthritis [4], ocular neovascularization [5], psoriasis [6], tumor growth [7] and metastasis [8]. Vascular endothelial growth factor (VEGF) and its receptor tyrosine kinases VEGFR-1 (Flt-1) and VEGFR-2 (KDR) are critical regulators of angiogenesis [9]. It is also important that the specific binding of VEGF to vascular cell surface expressed VEGFR-2 triggers effective downstream cell proliferation signaling pathways and leads to tumor vascularization [10,11]. The blockage of VEGFR-2 signaling by small molecule inhibitors to the VEGFR-2 kinase domain has been shown to inhibit angiogenesis, tumor progression, and dissemination in a number of preclinical and clinical studies [12–16]. Therefore, inhibition of the VEGFR-2 has become an attractive strategy in the treatment of cancers [17].

In recent years, several successful strategies for the inhibition of angiogenesis have been effectively demonstrated in preclinical

and clinical settings. For examples, the use of the neutralizing monoclonal antibody to VEGF, bevacizumab (Genentech), has demonstrated a prolonged survival in colorectal cancer patients [17]. In addition, small molecule inhibitors of KDR, such as sunitinib (SU-11248) and sorafenib (Bay 43-9006, 2; a dual raf-KDR inhibitor) have been approved very effective for the treatment of cancers [18–24]. Up to now, there are still a lot of researches focusing on the development of novel inhibitors of KDR [25–32]. Recently, a novel series of KDR inhibitors which can selectively inhibit KDR with high inhibitory activities reported by Harmange et al. [33–35].

In the present work, molecular modeling studies of these novel VEGFR-2 (KDR) inhibitors [33–35] were performed using 3D-QSAR and docking approach. Three-dimensional quantitative structure–activity relationship (3D-QSAR) methods, such as comparative molecular field analyses (CoMFA) [36,37] and comparative molecular similarity indices analyses (CoMSIA) [38], were applied to these inhibitors to gain insights into how steric, electrostatic, hydrophobic, and hydrogen-bonding interactions influence their activities. Docking study was performed to explore the binding mode between all of the compounds and the KDR, which produced the bioactive conformer of the whole dataset. To construct more reasonable 3D-QSAR models, we adopted two different conformer-based alignment methods. The results indicated that the models based on the docked conformer performed better than that based on the co-crystallized conformer. The constructed models can not only be used in rapidly and accurately predicting the activities

\* Corresponding author. Tel.: +86 931 891 2578; fax: +86 931 891 2582.

E-mail address: [xjyao@lzu.edu.cn](mailto:xjyao@lzu.edu.cn) (X. Yao).

of newly designed agonists, but also provide some beneficial information in structural modifications for designing new inhibitors with desired inhibitory activity.

## 2. Computational details

### 2.1. Dataset

A dataset of 82 compounds, which covered nearly four log units ( $\text{pIC}_{50} = 5.8\text{--}9.7$ ) for their inhibitory activity, was taken from the published KDR inhibitors [33–35]. The structures and their inhibitory activities are listed in Table 1. The inhibitory activity  $\text{IC}_{50}$  values (nM) against KDR were converted to the corresponding  $\text{pIC}_{50}$  ( $-\log \text{IC}_{50}$ ) and used as dependent variables in the CoMFA and CoMSIA analyses. The whole dataset was randomly divided into a training set of 63 compounds and a test set of 19 compounds (asterisked molecules in Table 1). The training set was used to construct 3D-QSAR models and the test set was used for the models validation.

### 2.2. Molecular modeling

All the molecular modeling and calculations were performed by SYBYL 6.9 molecular modeling package [39] on a Silicon Graphics O2 workstation running under the IRIX 6.5 operating system. Compound 10 in the X-ray crystal structure (3B8Q) [33] was used as the basic skeleton to obtain the structures of other compounds. Energy minimization process was performed using the MMFF94 force field with a distance-dependent dielectric and Powell gradient algorithm with a convergence criterion of 0.01 kcal/mol. Partial atomic charges were calculated using MMFF94 method.

In the 3D-QSAR studies, alignment rule and biological conformation selection are two important factors to construct reliable models. In the present study, two conformer-based alignment methods were employed. First, the co-crystallized conformer-based alignment (CCBA) was adopted. Compound 10 in the X-ray crystal structure (3B8Q) has been used to sketch the other compounds. Second, the docked conformer-based alignment (DCBA) was employed to align all of the compounds by considering the binding mode of these inhibitors to the receptor. Compound 10 was selected as a template for the alignment. Considering the structural difference of the two section of the whole dataset, 12 common atoms of compounds 1–60 and 13 common atoms of compounds 61–82 were selected for alignment. Molecules alignment was performed using DATABASE

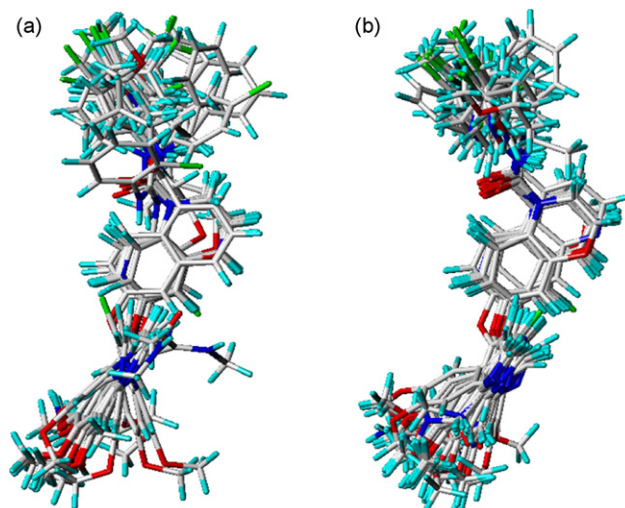


Fig. 2. Comparison of conformational alignments. (a) Co-crystallized conformer-based alignment (CCBA). (b) Docked conformer-based alignment (DCBA).

ALIGNMENT in SYBYL with the common substructure asterisked in compound 10 (Fig. 1(a) and (b)). The alignment results based on the two strategies were shown in Fig. 2(a) and (b).

### 2.3. Molecular docking

To determine the probable binding conformations of these inhibitors, the FlexX program [40] interfaced with SYBYL 6.9 was used to dock all the compounds into the active site of the KDR (PDB code: 3B8Q). FlexX is a fast automated docking program that considers ligand conformational flexibility by an incremental fragment placing technique [40]. The inhibitor and water molecules from crystal structure were removed, and hydrogen atoms were added. The active site for docking was defined as all atoms within 6.5 Å radius of the co-crystallized ligand. The default parameters in the FlexX module were used.

### 2.4. CoMFA and CoMSIA models generation

In deriving the CoMFA and CoMSIA descriptor fields, the  $\text{sp}^3$  carbon probe atom with a +1 charge and van der Waals radius of 1.52 Å was employed to calculate the CoMFA descriptors, steric

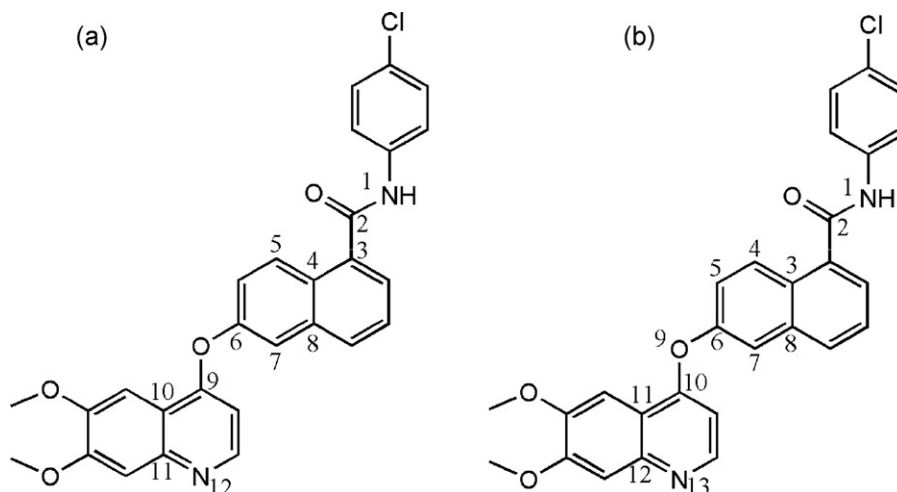
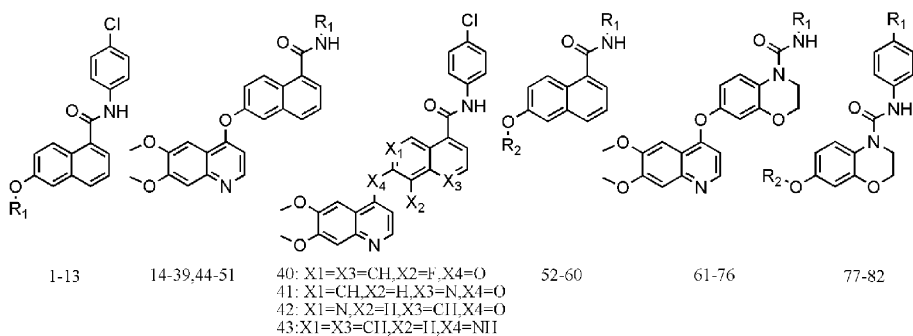


Fig. 1. Common atoms used for alignment. (a) Common atoms of compounds 1–60. (b) Common atoms of compounds 61–82.

**Table 1**

Dataset used for 3D-QSAR analysis with corresponding experimental and predicted activities.



NO.	R <sub>1</sub>	pIC <sub>50</sub> Exp.	CoMFA model		CoMSIA model	
			Pred.	Error	Pred.	Error
1		8.52	8.46	0.06	8.50	0.02
2		7.74	7.08	0.66	7.46	0.28
3*		8.15	7.00	1.15	7.55	0.60
4		6.51	6.58	-0.07	6.85	-0.34
5		7.34	7.32	0.02	7.36	-0.02
6		7.70	7.72	-0.02	7.78	-0.08
7*		7.55	7.50	0.05	7.43	0.12
8		8.40	8.39	0.01	8.63	-0.23
9		9.00	8.88	0.12	8.90	0.10

Table 1 (Continued)

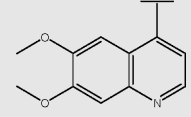
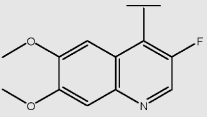
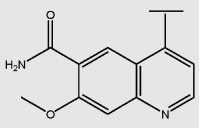
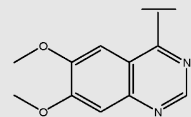
NO.	R <sub>1</sub>	pIC <sub>50</sub>				
		Exp.	CoMFA model		CoMSIA model	
			Pred.	Error	Pred.	Error
10		9.31	9.31	0.00	9.17	0.14
11		7.70	7.55	0.15	7.86	−0.16
12 <sup>+</sup>		9.70	9.42	0.28	9.00	0.70
13		8.70	8.38	0.32	8.45	0.25
	R <sub>1</sub>					
14	Ph	9.70	9.79	−0.09	9.99	−0.29
15	2-F-Ph	8.70	9.19	−0.49	8.96	−0.26
16 <sup>+</sup>	3-F-Ph	9.22	9.29	−0.07	8.85	0.37
17 <sup>+</sup>	4-F-Ph	9.00	9.23	−0.23	8.96	0.04
18 <sup>+</sup>	3-Cl-Ph	9.52	8.83	0.69	8.78	0.74
19	4-Me-Ph	9.30	9.11	0.19	9.21	0.09
20	3-CF <sub>3</sub> -Ph	9.30	9.20	0.10	9.21	0.09
21 <sup>+</sup>	4-CF <sub>3</sub> -Ph	9.30	9.30	0.00	9.18	0.13
22 <sup>+</sup>	4- <i>t</i> -Bu-Ph	9.15	9.13	0.02	9.00	0.16
23	2,4-Cl-Ph	8.70	8.67	0.03	8.74	−0.04
24	3,5-Cl-Ph	9.52	9.44	0.08	9.44	0.08
25	3-CF <sub>3</sub> -4-Cl-Ph	9.00	9.03	−0.03	9.08	−0.08
26	2-Pyridyl	9.10	9.06	0.04	9.02	0.08
27	3-Pyridyl	9.10	9.06	0.04	9.03	0.07
28	4-Pyridyl	8.70	8.78	−0.08	8.71	−0.01
29 <sup>+</sup>	2-Thiazolyl	9.52	8.88	0.64	9.09	0.43
30	3-Isoxazole	9.70	9.58	0.12	9.28	0.42
31	5-Methyl-3-isoxazolyl	9.22	9.55	−0.33	9.53	−0.31
32	3-Methyl-5-isoxazolyl	9.00	9.12	−0.12	8.94	0.06
33	5- <i>tert</i> -Butyl-3-isoxazolyl	9.10	8.86	0.24	9.28	−0.18
34	Cyclopropyl	9.22	9.13	0.09	9.37	−0.15
35	1-Methylcyclopropyl	7.82	7.56	0.26	8.00	−0.18
36	Cyclobutyl	8.67	8.75	−0.08	8.31	0.36
37	Cyclopentyl	7.92	7.93	−0.01	7.97	−0.05
38	Propyl	8.89	8.87	0.02	8.77	0.12
39	Isopropyl	8.26	7.91	0.36	8.19	0.07
40		9.52	9.57	−0.05	9.75	−0.23
41		7.66	7.89	−0.23	7.74	−0.08
42		7.64	7.58	0.06	7.61	0.03
43 <sup>+</sup>		8.10	7.98	0.13	7.80	0.30
	R <sub>1</sub>					
44 <sup>+</sup>	Cyclopropylmethyl	7.96	8.43	−0.47	8.32	−0.36
45	Methyl	8.42	8.60	−0.18	8.85	−0.43
46 <sup>+</sup>	Ethyl	8.89	8.87	0.02	9.17	−0.28
47	<i>t</i> -Butyl	5.82	6.74	−0.92	5.89	−0.07
48	2-Trifluoroethyl	8.42	8.24	0.19	8.16	0.27
49 <sup>+</sup>	2-Methoxyethyl	7.92	7.91	0.01	7.07	0.85
50	3-Methoxypropyl	8.38	8.56	−0.18	8.42	−0.04
51 <sup>+</sup>	H	9.05	8.74	0.31	9.00	0.05
	R <sub>1</sub>					
	R <sub>2</sub>					

Table 1 (Continued)

	R <sub>1</sub>	R <sub>2</sub>					
52	Cyclopropyl		8.54	8.28	0.26	8.41	0.13
53	2-Methoxyethyl		6.50	6.67	−0.17	6.52	−0.02
54*	H		8.89	8.93	−0.04	8.98	−0.09
55	Cyclopropyl		9.35	9.11	0.24	9.12	0.23
56	2-Methoxyethyl		7.55	7.79	−0.24	7.55	0.00
57	H		8.92	9.02	−0.10	9.13	−0.21
58	Cyclopropyl		9.43	9.40	0.03	9.44	−0.01
59	2-Methoxyethyl		7.66	7.54	0.13	7.57	0.09
60	H		8.89	8.92	−0.03	8.86	0.04
	R <sub>1</sub>						
61*	Ph		9.00	8.92	0.08	8.85	0.15
62	2-Me-Ph		9.00	8.75	0.25	8.89	0.11
63	3-Me-Ph		9.00	8.96	0.04	9.06	−0.06
64	4-Me-Ph		9.70	9.45	0.25	9.24	0.46
65	2-Cl-Ph		7.72	7.73	−0.01	7.76	−0.04
66	3-Cl-Ph		9.00	9.05	−0.05	9.04	−0.04
67	4-Cl-Ph		9.30	9.10	0.20	9.10	0.20
68	4-F-Ph		8.52	9.14	−0.62	8.81	−0.29
69	H		7.24	7.35	−0.11	7.27	−0.02
70	Methyl		7.40	7.48	−0.08	7.25	0.15
71*	Ethyl		9.00	8.10	0.90	8.17	0.83
72	<i>i</i> -Propyl		7.40	7.41	−0.01	7.38	0.03
73	Bn		7.28	7.26	0.02	7.31	−0.03
74*	4-Me-Bn		7.59	8.36	−0.77	7.59	0.00
75	(S)-Me-Bn		9.00	8.99	0.02	7.38	1.63
76	(R)-Me-Bn		7.40	7.27	0.13	7.31	0.09
	R <sub>1</sub>	R <sub>2</sub>					
77	Cl		9.22	9.48	−0.25	9.17	0.05
78	Me		9.30	9.38	−0.08	9.22	0.08
79	Cl		7.11	7.24	−0.13	7.28	−0.17
80	Me		7.59	7.61	−0.02	7.70	−0.11
81	Cl		7.02	6.92	0.10	6.87	0.15
82*	Me		7.21	6.97	0.24	6.80	0.41

\* Test set.

(Lennard–Jones potentials) and electrostatic (Coulomb potentials) field energies. The molecules were consistently aligned within the lattice that extended 4 Å units beyond the aligned molecules in all directions with a grid step size of 2 Å. The cutoff value of 30 kcal/mol was adopted. CoMSIA similarity index descriptors, namely steric, electrostatic, hydrophobic, hydrogen-bond donor and acceptor fields, were calculated using the sp<sup>3</sup> carbon probe atom with a +1 charge atom and a radius of 1.0 Å. In general, CoMSIA similarity indices  $A_{F,k}$  between the compounds of interest were

computed by placing a probe atom at the intersections of the lattice points using the following:

$$A_{F,k}^q(j) = - \sum_{i=1}^n w_{\text{probe},k} w_{ik} e^{-\alpha r_{iq}^2}$$

where  $q$  represents a grid point;  $i$  is summation index overall atoms of the molecule  $j$  under computation;  $w_{ik}$  is the actual value of physicochemical property  $k$  of atom  $i$ ;  $w_{\text{probe},k}$  is the value of the

probe atom. In present study, similarity indices were computed using a probe atom ( $w_{\text{probe},k}$ ) with charge +1, radius 1 Å, hydrophobicity +1. The attenuation factor was varied in a parameter study within the range from 0.1 to 0.9 in steps of 0.1 for the Gaussian-type distance. The statistical evaluation for the CoMSIA analyses was performed in the same way as described for CoMFA.

### 2.5. PLS regression analysis and models validation

To quantify the relationship between the structural descriptors (CoMFA and CoMSIA interaction energies) and the biological activities, partial least squares (PLS) regression analyses were used to derive 3D-QSAR models using the standard implementation in the SYBYL package. The CoMFA and CoMSIA descriptors were used as independent variables, and  $\text{pIC}_{50}$  values were used as the target variables. Cross-validation in PLS was carried out using the leave-one-out method to obtain the optimal number of components. The final model was constructed with the optimum number of components equal to that yielding to the highest  $q^2$ . In addition, the statistical significance of the models was described by the standard error of estimate (SEE), F and probability value computed according to the definitions in SYBYL. Column filtering thresholds of 2.0 kcal/mol for both CoMFA and CoMSIA was employed to shorten the computational time and to reduce the background noise. To further assess the robustness and statistical confidence of the derived models, bootstrapping [37,41] analysis for 100 runs was performed. Bootstrapping involves the generation of many new datasets from the original datasets after randomly choosing samples from the original dataset. A test set of molecules with known biological activities that were not included in the model generation was used to further validate the obtained models.

## 3. Results and discussion

### 3.1. Docking analysis

To determine the probable binding conformations of these inhibitors, FlexX was used to dock all compounds into the active sites of KDR. The docking reliability was validated using the known

X-ray structure of KDR in complex with a small molecular ligand. The compound 10 was re-docked to the binding site of protein and the docked conformation corresponding to the lowest free energies was selected as the most possible binding conformation. The root-mean-square deviation (RMSD) of the docked conformation to the experimental conformation was 0.69 Å, suggesting the high reliability of FlexX in reproducing the experimentally observed binding mode for these KDR inhibitors. Just as shown in Fig. 3(a), the co-crystallized 10 and redocked 10 are almost at the same position in the active sites of KDR. Therefore, the FlexX method was used to search the KDR binding conformations for other inhibitors.

Fig. 3(b) shows the 3D model of the 82 compounds at the active site of KDR. All of the inhibitors bound in the active site of KDR are in a similar conformation to ligand 10 in the X-ray structure co-crystallized with KDR. Based on the set of binding conformations and their alignment, CoMFA and CoMSIA were performed.

Compound 12, the most active compound among the whole dataset, was selected for detailed analysis. The best possible binding mode of compound 12 at the KDR active site and the main residues involved in the interaction were displayed in Fig. 3(c) and corresponding 2D representation of the interaction mode was presented in Fig. 3(d). Compound 12 binds to the active sites and forms several interactions with the hinge-binding region of the kinase. It can be seen clearly from Fig. 3(c) and (d) that the nitrogen atom of the quinoline ring of compound 12 forms an H-bond with the Cys919-NH in the kinase hinge region. In addition, the carbonyl and NH groups of the amide have two interactions with the backbone NH of Asp1046 and the side chain of Glu885, respectively, which is a typical characteristic of the interaction between the inhibitors and the “inactive” conformation of kinase. Moreover, compound 12 is surrounded by residues Leu840, Val848, Ala866, Lys868, Leu889, Thr916, Phe918, Gly922, Leu1035 and Phe1047 mainly through the hydrophobic interaction.

### 3.2. CoMFA and CoMSIA models

#### 3.2.1. CoMFA analysis

The best model for the alignment of compounds was selected based on the PLS statistical analysis. The statistical results for CoMFA

**Table 2**  
The statistical parameters for the final CoMFA and CoMSIA model.

Statistical parameters	CCBA model		DCBA model	
	CoMFA model		CoMSIA model	
	S + E	S + E + H + D + A	S + E	S + E + H + D + A
$r^{2a}$	0.898	0.934	0.936	0.961
SEE <sup>b</sup>	0.300	0.244	0.239	0.188
$F_{\text{test}}^c$	100.695	132.445	165.830	229.016
$q^{2d}$	0.484	0.711	0.546	0.715
$r^2_{\text{pred}}^e$	0.263	0.433	0.673	0.797
PLS components <sup>f</sup>	5	6	5	6
Contribution				
Steric	0.462	0.087	0.465	0.074
Electrostatic	0.538	0.297	0.535	0.250
Hydrophobic		0.236		0.284
Donor		0.167		0.204
Acceptor		0.213		0.188
$r^2_{\text{boot}}^g$	0.930 ± 0.019	0.949 ± 0.015	0.963 ± 0.014	0.956 ± 0.013
SEE <sub>boot</sub> <sup>h</sup>	0.246 ± 0.126	0.210 ± 0.107	0.177 ± 0.107	0.196 ± 0.108

<sup>a</sup> Correlation coefficient.

<sup>b</sup> Standard error of estimate.

<sup>c</sup> Ratio of  $r^2$  explained to unexplained =  $r^2/(1 - r^2)$ .

<sup>d</sup> Cross-validated correlation coefficient after leave-one-out procedure.

<sup>e</sup> Predicted correlation coefficient for test set of compounds.

<sup>f</sup> Optimal number of principal components.

<sup>g</sup> Average of correlation coefficient for 100 samplings using bootstrapped procedure.

<sup>h</sup> Average standard error of estimate for 100 samplings using bootstrapped procedure.



and CoMSIA models are summarized in Table 2. Both for CoMFA and CoMSIA analysis, the docked conformer-based alignment (DCBA) gave the best model. The best CoMFA model gave the cross-validated  $q^2$  of 0.546 with an optimal number of components (ONC) of 5 and a conventional correlation coefficient  $r^2$  of 0.936 for the non-cross-validated final model. The corresponding field contributions of steric and electrostatic are 46.5% and 53.5%. These values suggest a good conventional statistical correlation as shown in Fig. 4(a), and a satisfactory predictive ability of the CoMFA model.

### 3.2.2. CoMSIA analysis

CoMSIA models were generated using the combinations of the following fields: steric, electrostatic, hydrophobic, H-bond donor and H-bond acceptor. These descriptors illustrate the various properties into spatial locations where they play decisive roles in determining the biological activity. Computations of some possible combinations of different fields were performed in this study to determine the best CoMSIA model (Table 3). As a result, a combined use of all the five fields resulted in the best model. The attenuation factor  $\alpha$ , was also investigated. A series of  $\alpha$  were selected from 0.1 to 0.9 (see Fig. 5). Fig. 5 shows the changes of  $q^2$  of different 3D-QSAR

models with different  $\alpha$  values. For the dataset, the value of 0.3 gave the highest  $q^2$  value.

The best CoMSIA model gave the cross-validated  $q^2$  of 0.715, an optimal number of components (ONC) of 6 and a non-cross-validated coefficient  $r^2$  of 0.961. Fig. 4(b) shows the relationship between the predicted and the experimental  $\text{pIC}_{50}$  values for the non-cross-validated analysis of CoMSIA model. These values suggest a good conventional statistical correlation as shown in Fig. 4(b), and a satisfactory predictive ability of the CoMSIA model. The corresponding field contributions of variables are 7.4%, 25.0%, 28.4%, 20.4%, and 18.8%, respectively.

### 3.2.3. Validation of the 3D-QSAR models

To further assess the robustness and statistical confidence of the derived models, bootstrapping analysis for 100 runs was performed (Table 2). In all of the cases, higher values of  $r^2_{\text{boot}}$  were obtained which indicates the robustness of the models developed. The  $r^2_{\text{boot}}$  of 0.963 for CoMFA and 0.956 for CoMSIA suggests that a good internal consistency exists within the underlying dataset.

To validate the stability and predictive ability of the obtained models, 19 compounds not included in the construction of CoMFA and CoMSIA models were selected as the test set. The predicted

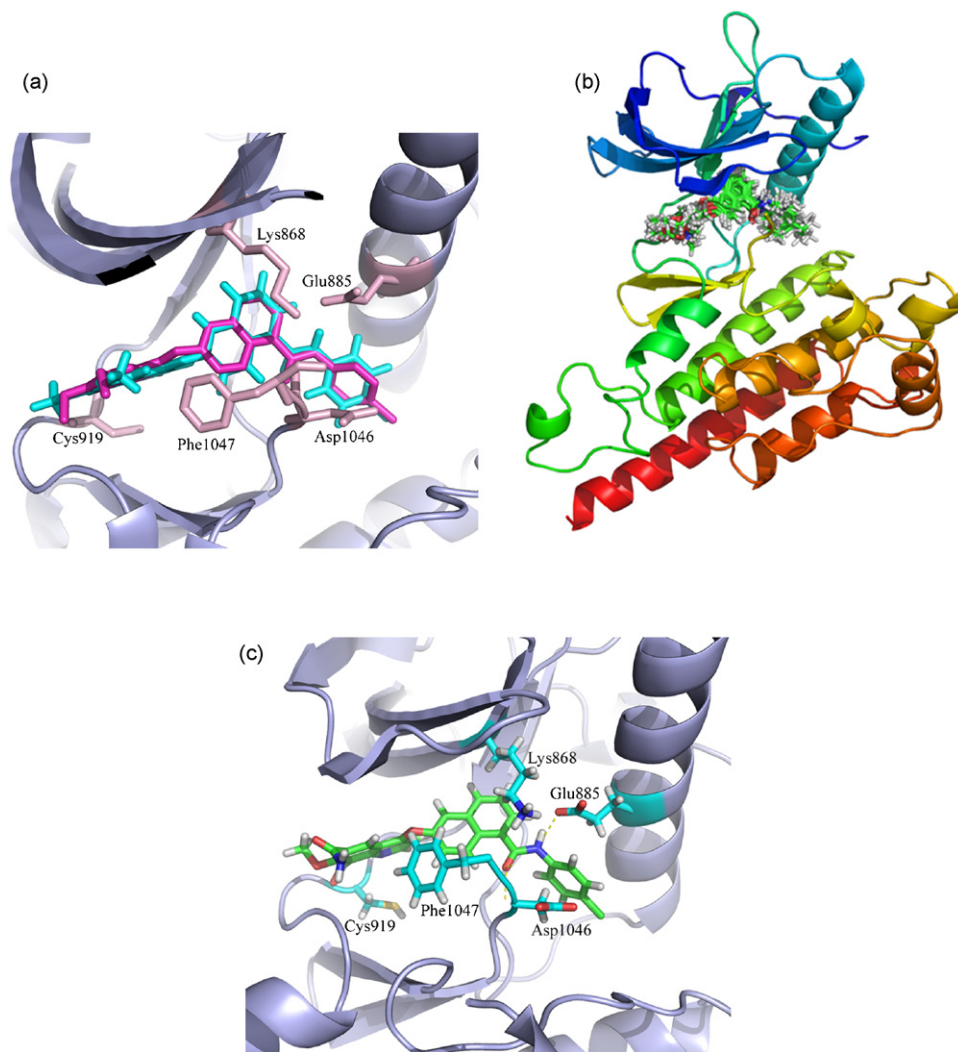


**Fig. 3.** (a) Binding conformations of the co-crystallized compound 10 and redocked compound 10 at the active sites of KDR produced using the PyMOL program [42]. Magenta compound represents co-crystallized compound 10 and Cyan compound represents redocked compound 10. (b) Binding conformations of docked compounds at the active sites of KDR. (c) Compound 12 docked in the binding pocket of KDR. (d) Schematic representation of interactions between compound 12 and the KDR produced using the Ligplot program developed by Wallace et al. [43].

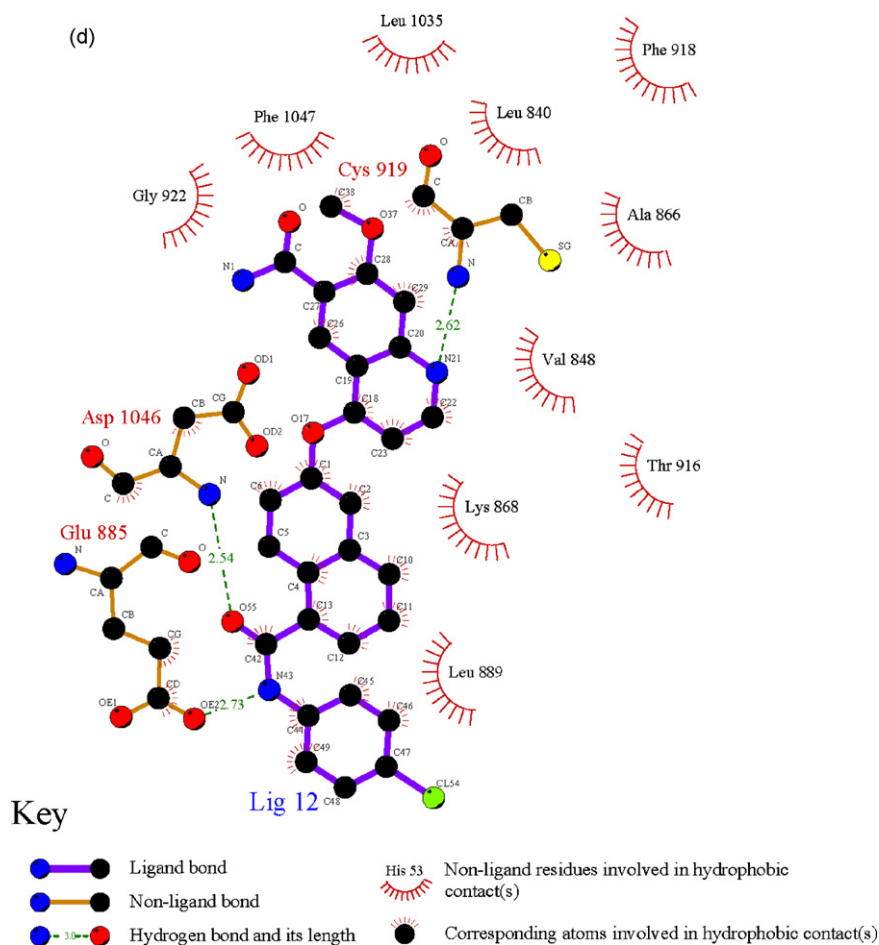


Fig. 3. (Continued).

results of the test set were also listed in Table 1 (asterisk labeled) and shown in Fig. 4. It can be seen clearly from Fig. 4 that the predicted  $\text{pIC}_{50}$  values of the test set compounds are in good agreement with the experimental data in a tolerable error range,

with  $r^2 = 0.673$  and  $0.797$  for CoMFA and CoMSIA models, respectively. Testing results indicate that the CoMFA and CoMSIA models could be reliably used to design novel inhibitors with desired activity for the KDR.

**Table 3**  
Summary of CoMSIA analysis.

Field(s)	$q^2$	ONC	$r^2$	SEE	$F$ ( $F$ -ratio)	$r^2_{\text{pred}}$	Contribution				
							$S$	$E$	$H$	$D$	$A$
$S^a$	0.484	5	0.795	0.426	44.276	0.482	1.000	–	–	–	–
$E^b$	0.489	3	0.795	0.419	76.309	0.501	–	1.000	–	–	–
$H^c$	0.682	5	0.855	0.358	67.242	0.766	–	–	1.000	–	–
$D^d$	0.314	4	0.561	0.618	18.503	0.434	–	–	–	1.000	–
$A^e$	0.181	4	0.509	0.654	15.037	0.234	–	–	–	–	1.000
SH	0.680	5	0.875	0.332	80.096	0.746	0.224	–	0.776	–	–
EH	0.674	6	0.930	0.251	124.394	0.741	–	0.511	0.489	–	–
HD	0.662	6	0.872	0.339	63.736	0.775	–	–	0.590	0.410	–
HA	0.626	6	0.919	0.270	105.842	0.782	–	–	0.681	–	0.319
SEH	0.710	5	0.930	0.250	150.704	0.743	0.135	0.438	0.427	–	–
SHD	0.691	6	0.899	0.302	82.889	0.747	0.138	–	0.511	0.351	0.000
SHA	0.669	5	0.917	0.271	125.647	0.802	0.166	–	0.509	–	0.325
EHD	0.672	6	0.928	0.256	119.409	0.781	–	0.352	0.385	0.263	–
SEHD	0.709	6	0.939	0.235	142.805	0.783	0.097	0.321	0.347	0.235	–
SEHA	0.724	6	0.959	0.191	220.878	0.773	0.104	0.333	0.337	–	0.226
SEHDA <sup>f</sup>	0.715	6	0.961	0.188	229.016	0.797	0.074	0.250	0.284	0.204	0.189

<sup>a</sup> Hydrophobic field.

<sup>b</sup> Hydrogen-bond donor field.

<sup>c</sup> Hydrogen-bond acceptor field.

<sup>d</sup> Steric field.

<sup>e</sup> Electrostatic field.

<sup>f</sup> Best model for CoMSIA.



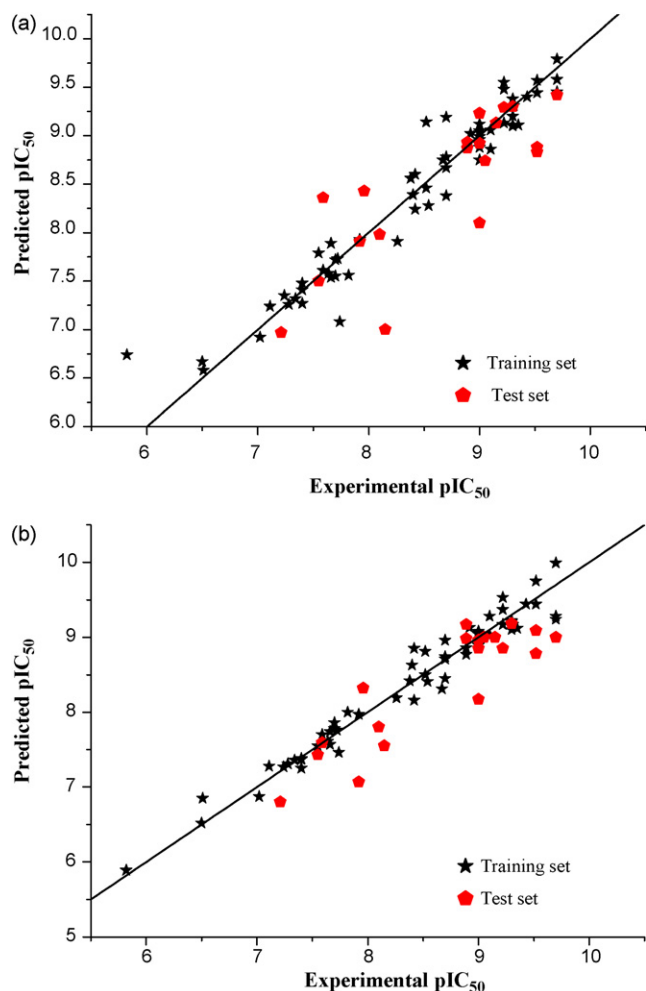


**Fig. 4.** Plot of the predicted  $pIC_{50}$  vs. the experimental  $pIC_{50}$  values for the CoMFA model (a) and CoMSIA model (b).

### 3.2.4. CoMFA and CoMSIA contour maps

Based on the best CoMFA and CoMSIA model, the  $S.D. \times \text{coeff}$  contour maps were constructed. The contour maps superimposed at the active site of the KDR usually provide a more detailed

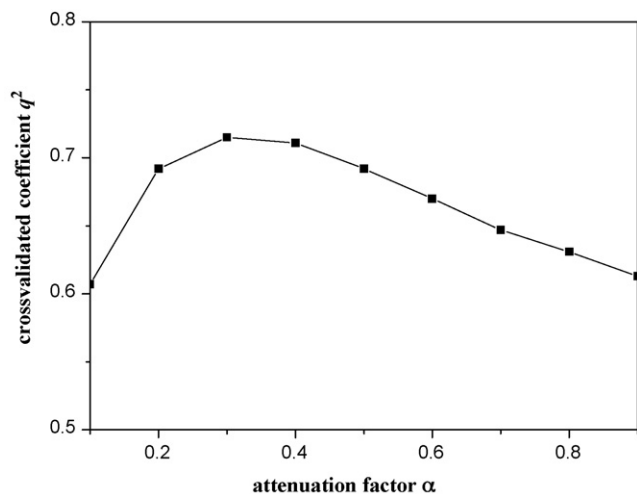


**Fig. 5.** Variations of  $q^2$  upon changes of the attenuation factor  $\alpha$  used in the distance dependence between the probe atom and the atoms of the molecules in CoMSIA.

understanding of the key structural features required for the biological activity. For better visualization, some unimportant residues are not shown in constructed contour maps.

The CoMFA contour maps of steric and electrostatic field superimposed at the active site of the KDR are shown in Fig. 6. In the CoMFA steric field, the green contours (contribution level of 80%) represent a steric group that confers an increased activity while yellow contours (contribution level of 20%) represent a bulky group that results in a decreased activity. Similarly the blue contours indicate regions where the addition of electropositive substituents increases activity (contribution level of 80%); red contours indicate regions where the addition of electronegative substituents increases activity (contribution level of 20%). Compound 10 is displayed in the map in aid of visualization.

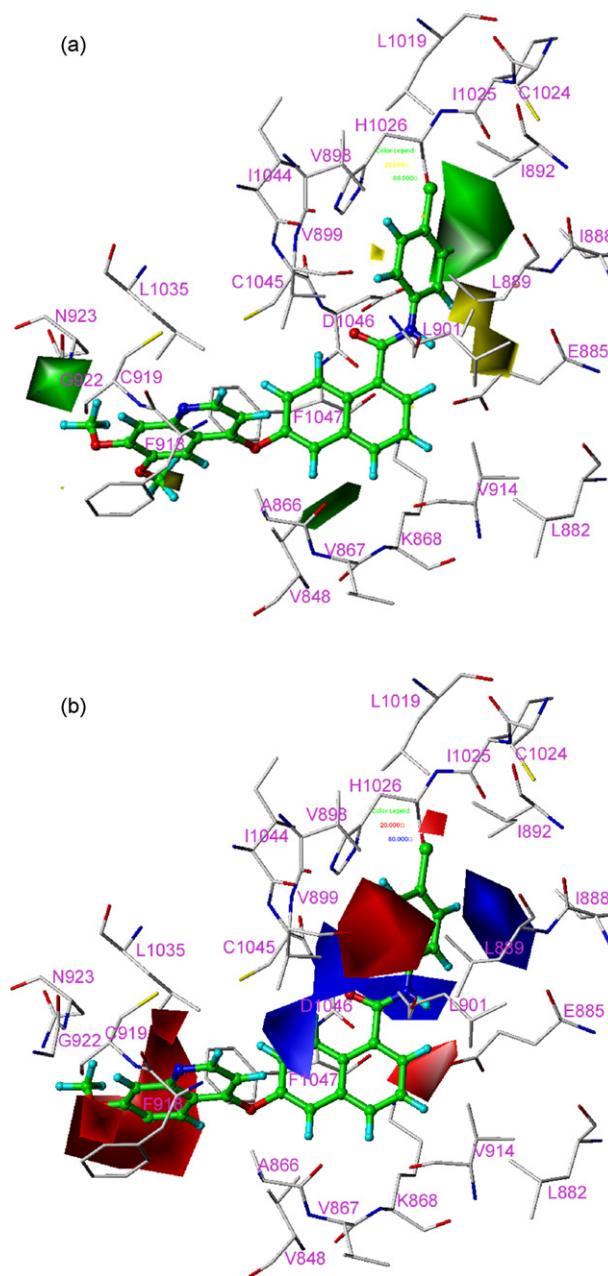


**Fig. 6.** CoMFA  $S.D. \times \text{coeff}$  contour plots. (a) Contour maps for steric field: favored (green), disfavored (yellow). (b) Contour maps for black electrostatic field: electropositive (blue), electronegative (red).

In Fig. 6(a), the contour map of the steric field of CoMFA model, a large region of green contour near the 3'-positions of 1-phenyl in compound 10 suggest that bulky group would increase the activity. Two moderate regions of yellow contours near the residue Leu889 indicate that steric bulk is disfavored there. It can explain the fact that the activity of compound 15 is lower than that of compound 14. It can also explain the poor inhibitory activities of the compounds 35, 37, 39 and 47 with bulky alkyl groups at 1-position. From the docking study, it can be seen that this area is blocked by Leu889. A small region of green contour around the quinoline ring in compound 10 suggests that steric bulk is favored there. In consistent with this, the compounds with bulky groups at this position such as compounds 9, 10, 12, 13, have higher activity,

while the compounds 1–6 with small groups at the same position showed lower activity.

In the contour map of the electrostatic field of CoMFA model, shown in Fig. 6(b), a blue contour around the 3'-position of the 1-phenyl indicates that electropositive substituents are favored there. A red area near the 6'-position of the 1-phenyl ring suggests that electronegative substituents are favored there. A region of blue contour near the naphthyl ring suggests that electropositive substituents would increase the activity. An alternative approach involved the incorporation of a heteroatom into the naphthyl ring resulted in the decreased activities (compounds 41 and 42). A large red area near the quinoline ring in compound 10 indicates that electronegative substituents are favored there. Compounds 64, 67,

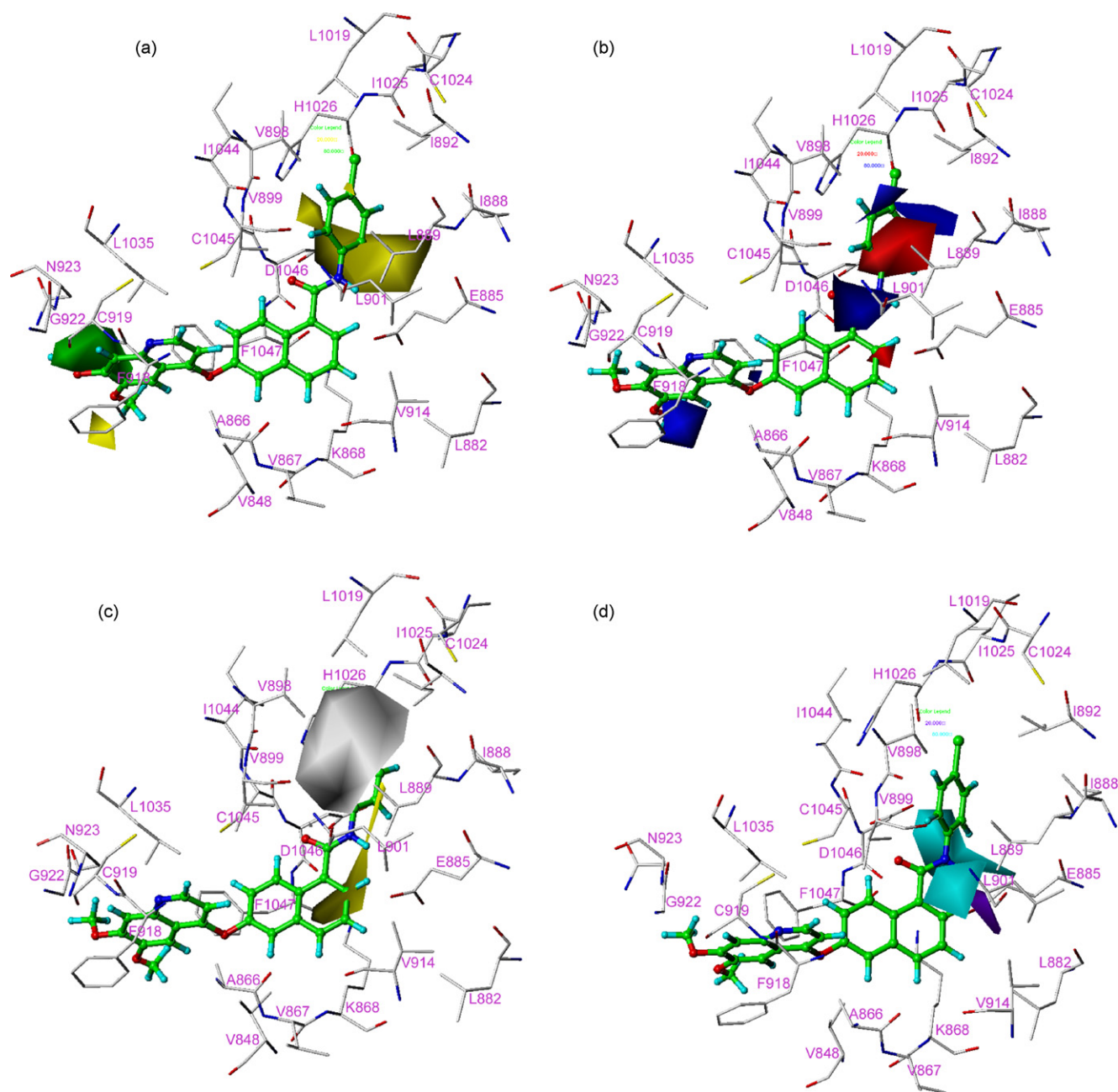


**Fig. 7.** CoMSIA S.D.  $\times$  coeff contour plots. (a) Contour maps for steric field: favored (green), disfavored (yellow). (b) Contour maps for electrostatic field: electropositive (blue), electronegative (red). (c) Contour maps for hydrophobic field: favored (yellow), disfavored (white). (d) Contour maps for H-bond donor field: favored (cyan), disfavored (purple). (e) Contour maps for H-bond acceptor field: favored (magenta), disfavored (red).

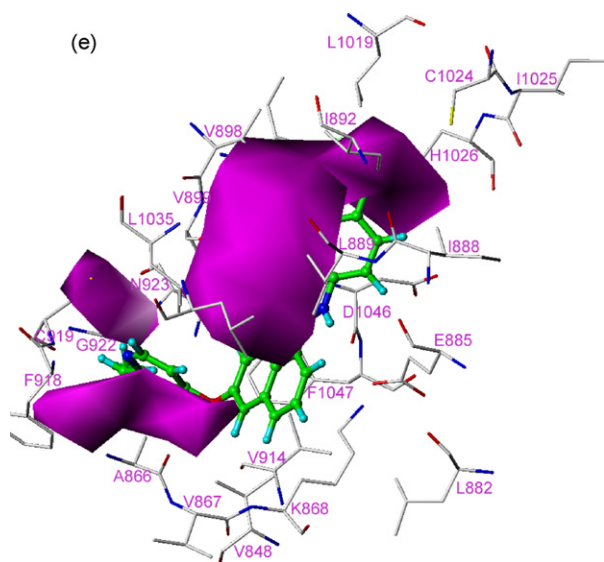


Fig. 7. (Continued).

77 and 78 with electronegative substituents at this position showed superior activities than that of compounds 79–82.

Fig. 7(a) and (b) describes the steric and electrostatic contour maps of the CoMSIA models. These contours are almost similar to the CoMFA-steric and electrostatic contours (Fig. 6(a) and (b)). Therefore, our following discussion will focus on the other three fields, hydrophobic, hydrogen-bond donor and hydrogen-bond acceptor fields. The hydrophobic contour map of CoMSIA model is displayed in Fig. 7(c). Yellow (contribution level of 80%) and gray (contribution level of 20%) contours indicate the regions where hydrophobic and hydrophilic groups were preferred, respectively. A moderate yellow contour map around the naphthyl ring indicates that hydrophobic groups would be favorable for binding activity. This yellow contour is surrounded by the residues Val848, Ala866, Val867, Lys868 and Val914, which formed a moderately hydrophobic binding pocket in KDR. The large gray contour map located around the 4'-, 5'-, 6'-positions of 1-phenyl ring in compound 10 suggest that hydrophobic groups at these positions would decrease the binding affinity.

The CoMSIA contour map of the hydrogen-bond donor and hydrogen-bond acceptor field are shown in Fig. 7(d) and (e), respectively. Cyan contours (contribution level of 80%) indicate regions where H-bond donor group increases activity, purple

contours (contribution level of 20%) suggest regions where H-bond donor group decreases activity. Two cyan contour near the amide group suggest that H-bond donor groups are favored there, which is consistent well with the results of the docking study that the NH group in this region forms a hydrogen-bond with Glu885 as hydrogen donor. In Fig. 7(e), Magenta contours (contribution level of 80%) indicate regions where H-bond acceptor group increases activity; red contours (contribution level of 20%) represent region where H-bond acceptor group decreases activity. A large magenta contour near the carbonyl group indicates that H-bond acceptor groups are favored there. The docking study showed that the carbonyl group forms a hydrogen-bond with Asp1046. Two moderate magenta contours near the quinoline ring suggest H-bond acceptor groups are preferred there. As docking study showed, the nitrogen atom of the quinoline ring formed H-bond with Cys919 as acceptor.

### 3.3. Designing of potent analogs

According to the detailed contour analyses of both CoMFA and CoMSIA models as discussed in the previous section, several useful information on the structural requirements for the observed inhibitory activities were obtained. We have employed these information to design several analogs with improved activity. The most potent molecule (compound 14) was used as a reference structure to design new molecules. These new proposed compounds were generated by combining substituents on the positions 1, 2, and 3 of the basic skeleton of compound 14 and it was further evaluated that the way in which the tested changes affect the inhibitory activity. For this evaluation, the docked conformer-based alignment (DCBA) CoMSIA model was used since it demonstrated to be more robust than the other models. Three important substituent positions were identified and shown in Table 4. Firstly, Variations (R1, Table 4) were made on the 1-phenyl ring, at the para position. Secondly, Modifications (R2, Table 4) were also made at the naphthyl ring. It is seen that the molecules with R2 groups at the naphthyl ring with suitable substituents, are predicted with higher activity. Thirdly, variations (R3, Table 4) were made on the quinoline ring. Some of the newly designed molecules are depicted in Table 4.

## 4. Conclusion

In the present study, molecular docking and 3D-QSAR analysis have been successfully applied to a set of recently synthesized KDR inhibitors. Docking studies were employed to obtain the bioactive

**Table 4**  
Structures and predicted pIC<sub>50</sub> values of the designed compounds.

	Compound	R <sub>1</sub>	R <sub>2</sub>	R <sub>3</sub>	pIC <sub>50</sub> <sup>a</sup>
	new001	H	H	COOCH3	9.72
	new002	CF3	Cl	OCH3	9.82
	new003	CF3	Br	OCH3	9.81
	new004	CF3	I	OCH3	9.77
	new005	CF3	Cl	OC2H5	9.82
	new006	CF3	Cl	COOCH3	10.05
	new007	CF3	Br	COOCH3	10.03
	14	H	H	OCH3	9.99

<sup>a</sup> pIC<sub>50</sub> values predicted by the docked conformer-based alignment (DCBA) CoMSIA model.



conformer of the whole dataset. Two different conformer-based alignment methods were used to explore their impacts on the 3D QSAR model generation. Comparing the two conformer-based alignment methods, the docked conformer-based alignment (DCBA) model gave  $q^2$  and  $r^2$  values for CoMFA and CoMSIA of 0.546 and 0.936, 0.715 and 0.961, respectively, which were much better than those of the co-crystallized conformer-based alignment (CCBA) model. The effects of the steric, electrostatic, hydrophobic and H-bond donor and acceptor fields around the docked conformations on their activities were discussed in detail. Both docking studies and 3D-QSAR models provide useful information in understanding the structural features of the target and chemical features of the ligands. The information can also provided some useful information that can be used to design novel molecules with desired activity.

## Acknowledgement

This work was supported by the Program for New Century Excellent Talents in University (No. NCET-07-0399).

## Appendix A. Supplementary data

Supplementary data associated with this article can be found, in the online version, at doi:10.1016/j.jmgm.2008.10.006.

## References

- [1] W. Risau, Mechanisms of angiogenesis, *Nature* 386 (1997) 671–674.
- [2] D. Ribatti, A. Vacca, B. Nico, L. Roncali, F. Dammacco, Postnatal vasculogenesis, *Mech. Dev.* 100 (2001) 157–163.
- [3] G.A. Fava, Affective disorders and endocrine disease. New insights from psychosomatic studies, *Psychosomatics* 35 (1994) 341–353.
- [4] D.A. Walsh, L. Haywood, Angiogenesis: a therapeutic target in arthritis, *Curr. Opin. Invest. Drugs* 2 (2001) 1054–1063.
- [5] L.P. Aiello, R.L. Avery, P.G. Arrigg, B.A. Keyt, H.D. Jampel, S.T. Shah, L.R. Pasquale, H. Thieme, M.A. Iwamoto, J.E. Park, H.V. Nguyen, L.M. Aiello, N. Ferrara, G.L. King, Vascular endothelial growth factor in ocular fluid of patients with diabetic retinopathy and other retinal disorders, *N. Engl. J. Med.* 331 (1994) 1480–1487.
- [6] M. Detmar, The role of VEGF and thrombospondins in skin angiogenesis, *J. Dermatol. Sci.* 24 (2000) 78–84.
- [7] J. Folkman, Anti-angiogenesis: new concept for therapy of solid tumors, *Ann. Surg.* 175 (1972) 409–416.
- [8] L.A. Liotta, P.S. Steeg, W.G. Stetler-Stevenson, Cancer metastasis and angiogenesis: an imbalance of positive and negative regulation, *Cell* 64 (1991) 327–336.
- [9] L.K. Shawver, K.E. Lipson, T.A.T. Fong, G. McMahon, G.D. Plowman, L.M. Strawn, Receptor tyrosine kinases as targets for inhibition of angiogenesis, *Drug Discov. Today* 2 (1997) 50–63.
- [10] N. Ferrara, VEGF and the quest for tumour angiogenesis factors, *Nat. Rev. Cancer* 2 (2002) 795–803.
- [11] P. Carmeliet, R.K. Jain, Angiogenesis in cancer and other diseases, *Nature* 407 (2000) 249–257.
- [12] S. Baka, A.R. Clamp, G.C. Jayson, A review of the latest clinical compounds to inhibit VEGF in pathological angiogenesis, *Expert Opin. Ther. Targets* 10 (2006) 867–876.
- [13] L. Sepp-Lorenzino, K.A. Thomas, Antiangiogenic agents targeting vascular endothelial growth factor and its receptors in clinical development, *Expert Opin. Invest. Drugs* 11 (2002) 1447–1465.
- [14] B.M. Klebl, G. Müller, Second-generation kinase inhibitors, *Expert Opin. Ther. Targets* 9 (2005) 975–993.
- [15] C.T. Supuran, A. Scozzafava, Protein tyrosine kinase inhibitors as anticancer agents, *Expert Opin. Ther. Pat.* 14 (2004) 35–53.
- [16] K. Holmes, O.L. Roberts, A.M. Thomas, M.J. Cross, Vascular endothelial growth factor receptor-2: structure, function, intracellular signalling and therapeutic inhibition, *Cell. Signal.* 19 (2007) 2003–2012.
- [17] N. Ferrara, K.J. Hillan, H.P. Gerber, W. Novotny, Discovery and development of bevacizumab, an anti-VEGF antibody for treating cancer, *Nat. Rev. Drug Discov.* 3 (2004) 391–400.
- [18] K.M. Sakamoto, Su-11248 Sugan, *Curr. Opin. Invest. Drugs* 5 (2004) 1329–1339.
- [19] A.L. Thomas, B. Morgan, J. Dreves, C. Unger, B. Wiedenmann, U. Vanhoefer, D. Laurent, M. Dugan, W.P. Steward, Vascular endothelial growth factor receptor tyrosine kinase inhibitors: PTK787/ZK 222584, *Semin. Oncol.* 30 (2003) 32–38.
- [20] T. Ahman, T. Eisen, Kinase Inhibition with BAY 43-9006 in renal cell carcinoma, *Clin. Cancer Res.* 10 (2004) 6388–6392.
- [21] B. Ruggeri, J. Singh, D. Gingrich, T. Angeles, M. Albom, S. Yang, H. Chang, C. Robinson, K. Hunter, P. Dobrzanski, S. Jones-Bolin, S. Pritchard, L. Aimone, A. Klein-Szanto, J.M. Herbert, F. Bono, P. Schaeffer, P. Casellas, B. Bourie, R. Pili, J. Isaacs, M. Ator, R. Hudkins, J. Vaught, J. Mallamo, C. Dionne, CEP-7055: a novel, orally active pan inhibitor of vascular endothelial growth factor receptor tyrosine kinases with potent antiangiogenic activity and antitumor efficacy in preclinical models, *Cancer Res.* 63 (2003) 5978–5991.
- [22] J.S. Beebe, J.P. Jani, E. Knauth, P. Goodwin, C. Higdon, A.M. Rossi, E. Emerson, M. Finkelstein, E. Floyd, S. Harriman, J. Atherton, S. Hillerman, C. Soderstrom, K. Kou, T. Gant, M.C. Noe, B. Foster, F. Rastinejad, M.A. Marx, T. Schaeffer, P.M. Whalen, W.G. Roberts, Pharmacological characterization of CP-547,632, a novel vascular endothelial growth factor receptor-2 tyrosine kinase inhibitor for cancer therapy, *Cancer Res.* 63 (2003) 7301–7309.
- [23] A.J. Ryan, S.R. Wedge, ZD6474-a novel inhibitor of VEGFR and EGFR tyrosine kinase activity, *Br. J. Cancer* 92 (2005) 6–13.
- [24] A. Polverino, A. Coxon, C. Starnes, Z. Diaz, T. DeMelfi, L. Wang, J. Bready, J. Estrada, R. Cattley, S. Kaufman, D. Chen, Y. Gan, G. Kumar, J. Meyer, S. Neervannan, G. Alva, J. Talvenheimo, S. Montestruque, A. Tasker, V. Patel, R. Radinsky, R. Kendall, AMG 706, an oral, multitargeted inhibitor that selectively targets vascular endothelial growth factor, platelet-derived growth factor, and kit receptors, potentially inhibits angiogenesis and induces regression in tumor xenografts, *Cancer Res.* 66 (2006) 8715–8721.
- [25] A. Wissner, M.B. Floyd, B.D. Johnson, H. Fraser, C. Ingalls, T. Nittoli, R.G. Dushin, C. Discifani, R. Nilakantan, J. Marini, M. Ravi, K. Cheung, X. Tan, S. Musto, T. Annable, M.M. Siegel, F. Loganzo, 2-(Quinazolin-4-ylamino)-[1,4]benzoquinones as covalent-binding, irreversible inhibitors of the kinase domain of vascular endothelial growth factor receptor-2, *J. Med. Chem.* 48 (2005) 7560–7581.
- [26] R.S. Bhide, Z.W. Cai, Y.Z. Zhang, L. Qian, D. Wei, S. Barbosa, L.J. Lombardo, R.M. Borzilleri, X. Zheng, L.I. Wu, J.C. Barrish, S.H. Kim, K. Leavitt, A. Mathur, L. Leith, S. Chao, B. Wautlet, S. Mortillo, R. Jeyaseelan, D. Kukral, J.T. Hunt, A. Kamath, A. Fura, V. Vyas, P. Marathe, C. D'Arienzo, G. Derbin, J. Fargnoli, Discovery and preclinical studies of (R)-1-(4-(4-fluoro-2-methyl-1H-indol-5-yloxy)-5-methylpyrrolo[2,1-f][1,2,4]triazin-6-yloxy)propan-2-ol (BMS-540215), an in vivo active potent VEGFR-2 inhibitor, *J. Med. Chem.* 49 (2006) 2143–2146.
- [27] R.M. Borzilleri, R.S. Bhide, J.C. Barrish, C.J. D'Arienzo, G.M. Derbin, J. Fargnoli, J.T. Hunt, R. Jeyaseelan, A. Kamath, D.W. Kukral, P. Marathe, S. Mortillo, L. Qian, J.S. Tokarski, B.S. Wautlet, X. Zheng, L.J. Lombardo, Discovery and evaluation of N-cyclopropyl-2,4-difluoro-5-((2-(pyridin-2-ylamino)thiazol-5-ylmethyl)amino)-benzamide (BMS-605541), a selective and orally efficacious inhibitor of vascular endothelial growth factor receptor-2, *J. Med. Chem.* 49 (2006) 3766–3769.
- [28] M.H. Potashman, J. Bready, A. Coxon, T.M. DeMelfi, L. DiPietro, N. Doerr, D. Elbaum, J. Estrada, P. Gallant, J. Germain, Y. Gu, J.C. Harmange, S.A. Kaufman, R. Kendall, J.L. Kim, G.N. Kumar, A.M. Long, S. Neervannan, V.F. Patel, A. Polverino, P. Rose, S. vanderPlas, D. Whittington, R. Zanon, H. Zhao, Design, synthesis, and evaluation of orally active benzimidazoles and benzoxazoles as vascular endothelial growth factor-2 receptor tyrosine kinase inhibitors, *J. Med. Chem.* 50 (2007) 4351–4373.
- [29] M. Hasegawa, N. Nishigaki, Y. Washio, K. Kano, P.A. Harris, H. Sato, I. Mori, R.I. West, M. Shibahara, H. Toyoda, L. Wang, R.T. Nolte, J.M. Veal, M. Cheung, Discovery of novel benzimidazoles as potent inhibitors of TIE-2 and VEGFR-2 tyrosine kinase receptors, *J. Med. Chem.* 50 (2007) 4453–4470.
- [30] Z.-w. Cai, D. Wei, R.M. Borzilleri, L. Qian, A. Kamath, S. Mortillo, B. Wautlet, B.J. Henley, R. Jeyaseelan Sr., J. Tokarski, J.T. Hunt, R.S. Bhide, J. Fargnoli, L.J. Lombardo, Synthesis, SAR, and evaluation of 4-[2,4-difluoro-5-(cyclopropylcarbamoyl)phenylamino]pyrrolo[2,1-f][1,2,4]triazine-based VEGFR-2 kinase inhibitors, *Bioorg. Med. Chem. Lett.* 18 (2008) 1354–1358.
- [31] O. Ilovich, O. Jacobson, Y. Aviv, A. Litchi, R. Chisin, E. Mishani, Formation of fluorine-18 labeled diaryl ureas—labeled VEGFR-2/PDGFR dual inhibitors as molecular imaging agents for angiogenesis, *Bioorg. Med. Chem.* 16 (2008) 4242–4251.
- [32] R. Ruel, C. Thibeault, A. L'Heureux, A. Martel, Z.-W. Cai, D. Wei, L. Qian, J.C. Barrish, A. Mathur, C. D'Arienzo, J.T. Hunt, A. Kamath, P. Marathe, Y. Zhang, G. Derbin, B. Wautlet, S. Mortillo, R. Jeyaseelan Sr., B. Henley, R. Tejwani, R.S. Bhide, G.L. Trainor, J. Fargnoli, L.J. Lombardo, Discovery and preclinical studies of 5-isopropyl-6-(5-methyl-1,3,4-oxadiazol-2-yl)-N-(2-methyl-1H-pyrrolo[2,3-b]pyridin-5-yl)pyrrolo[2,1-f][1,2,4]triazin-4-amine (BMS-645737), an in vivo active potent VEGFR-2 inhibitor, *Bioorg. Med. Chem. Lett.* 18 (2008) 2985–2989.
- [33] J.-C. Harmange, M.M. Weiss, J. Germain, A.J. Polverino, G. Borg, J. Bready, D. Chen, D. Choquette, A. Coxon, T. DeMelfi, L. DiPietro, N. Doerr, J. Estrada, J. Flynn, R.F. Graceffa, P. Harriman, S. Kaufman, D.S. La, A. Long, M.W. Martin, S. Neervannan, V.F. Patel, M. Potashman, K. Regal, P.M. Roveto, M.L. Schrag, C. Starnes, A. Tasker, Y. Teffera, L. Wang, R.D. White, D.A. Whittington, R. Zanon, Naphthamides as novel and potent vascular endothelial growth factor receptor tyrosine kinase inhibitors: design, synthesis, and evaluation, *J. Med. Chem.* 51 (2008) 1649–1667.
- [34] M.M. Weiss, J.-C. Harmange, A.J. Polverino, D. Bauer, L. Berry, V. Berry, G. Borg, J. Bready, D. Chen, D. Choquette, A. Coxon, T. DeMelfi, N. Doerr, J. Estrada, J. Flynn, R.F. Graceffa, S.P. Harriman, S. Kaufman, D.S. La, A. Long, S. Neervannan, V.F. Patel, M. Potashman, K. Regal, P.M. Roveto, M.L. Schrag, C. Starnes, A. Tasker, Y. Teffera, D.A. Whittington, R. Zanon, Evaluation of a series of naphthamides as potent, orally active vascular endothelial growth factor receptor-2 tyrosine kinase inhibitors, *J. Med. Chem.* 51 (2008) 1668–1680.
- [35] D.S. La, J. Belzile, J.V. Bready, A. Coxon, T. DeMelfi, N. Doerr, J. Estrada, J.C. Flynn, S.R. Flynn, R.F. Graceffa, S.P. Harriman, J.F. Larrow, A.M. Long, M.W. Martin, M.J. Morrison, V.F. Patel, P.M. Roveto, L. Wang, M.M. Weiss, D.A. Whittington, Y. Teffera, Z. Zhao, A.J. Polverino, J.-C. Harmange, Novel 2,3-dihydro-1,4-benzoxazines as potent and orally bioavailable inhibitors of tumor-driven angiogenesis, *J. Med. Chem.* 51 (2008) 1695–1705.

- [36] R.D. Cramer 3rd, D.E. Patterson, J.D. Bunce, Comparative molecular field analysis (CoMFA). 1. Effect of shape on binding of steroids to carrier proteins, *J. Am. Chem. Soc.* 110 (1988) 5959–5967.
- [37] R.D. Cramer 3rd, J.D. Bunce, D.E. Patterson, Crossvalidation, bootstrapping, and partial least squares compared with multiple regression in conventional QSAR studies, *Quant. Struct.-Act. Relat.* 7 (1988) 18–25.
- [38] G. Klebe, U. Abraham, T. Mietzner, Molecular similarity indices in a comparative analysis (CoMSIA) of drug molecules to correlate and predict their biological activity, *J. Med. Chem.* 37 (1994) 4130–4146.
- [39] Sybyl version6.9, Tripos Associates, St. Louis, MO, 1999.
- [40] M. Rarey, B. Kramer, T. Lengauer, G. Klebe, A fast flexible docking method using an incremental construction algorithm, *J. Mol. Biol.* 261 (1996) 470–489.
- [41] L. Stahle, S. Wold, Multivariate data analysis and experimental design in biomedical research, *Prog. Med. Chem.* 25 (1988) 292–338.
- [42] W.L. DeLano, The PyMOL Molecular Graphics System DeLano Scientific, Palo Alto, CA, USA, 2002.
- [43] A.C. Wallace, R.A. Laskowski, J.M. Thornton, LIGPLOT: A program to generate schematic diagrams of protein–ligand interactions, *Prot. Eng.* 8 (1995) 127–134.